

Supplementary Information for “A universal gate for fixed-frequency qubits via a tunable bus”

David C. McKay,^{1, a)} Stefan Filipp,² Antonio Mezzacapo,¹ Easwar Magesan,¹ Jerry M. Chow,¹ and Jay M. Gambetta¹

¹⁾*IBM T.J. Watson Research Center, Yorktown Heights, NY 10598, USA*

²⁾*IBM Research - Zurich, 8803 Rueschlikon, Switzerland*

(Dated: 11 April 2016)

^{a)}Electronic mail: dcmckay@us.ibm.com

I. SYSTEM SETUP

All experiments are performed at $\approx 10\text{mK}$ in a dilution refrigerator with the line configurations illustrated in Fig. 1. The qubits and high speed flux line are driven with shaped microwave pulses sequenced by an arbitrary waveform generator (TEK5014C). To generate the drive for the high speed flux line (the tunable bus drive), the signals from the generators used for the single qubit gates are mixed down to ensure phase stability and appropriate timing across experiments. The qubit state is measured in the standard way by heterodyne detection of a microwave signal reflected off CPW readout resonators coupled to each qubit. These readout resonators are at 6.8696 GHz and 6.7838 GHz respectively.

II. HAMILTONIAN DERIVATION AND NUMERICS

To derive Eq. (6) from Eq. (3) in the main text, we expand the flux tunable dressed frequencies and exchange coupling,

$$\tilde{\omega}_i(\Phi) = \omega_i + \frac{g_i^2}{\Delta_i(\Phi)}, \quad (1)$$

$$J(\Phi) = \frac{g_1 g_2}{2} \left(\frac{1}{\Delta_1(\Phi)} + \frac{1}{\Delta_2(\Phi)} \right), \quad (2)$$

in the small parameter δ where $\Phi(t) = \Theta + \delta \cos(\omega_\Phi t)$. Expanding Eq. (1) to second-order,

$$\tilde{\omega}_i(\Phi(t)) \approx \tilde{\omega}_i(\Theta) + \left. \frac{\partial \tilde{\omega}_i}{\partial \Phi} \right|_{\Phi \rightarrow \Theta} \delta \cos(\omega t) + \frac{1}{2} \left. \frac{\partial^2 \tilde{\omega}_i}{\partial \Phi^2} \right|_{\Phi \rightarrow \Theta} (\delta \cos(\omega t))^2, \quad (3)$$

$$= \left[\tilde{\omega}_i(\Theta) - \frac{\delta^2}{4} \left. \frac{\partial^2 \tilde{\omega}_i}{\partial \Phi^2} \right|_{\Phi \rightarrow \Theta} \right] + \left. \frac{\partial \tilde{\omega}_i}{\partial \Phi} \right|_{\Phi \rightarrow \Theta} \delta \cos(\omega t) + \frac{\delta^2}{4} \left. \frac{\partial^2 \tilde{\omega}_i}{\partial \Phi^2} \right|_{\Phi \rightarrow \Theta} \cos(2\omega t), \quad (4)$$

there is a second-order DC shift and two oscillating terms. A similar expansion holds for the exchange term J . Numerical plots of the derivatives for $\tilde{\omega}$ and J that appear in these expansions are shown in Fig. 2. If the drive frequency ω_Φ is equal to the qubit detuning (including the DC drive-induced shifts), i.e.,

$$\omega_\Phi = (\tilde{\omega}_1(\Theta) - \tilde{\omega}_2(\Theta)) + \frac{\delta^2}{4} \left(\left. \frac{\partial^2 \tilde{\omega}_2}{\partial \Phi^2} \right|_{\Phi \rightarrow \Theta} - \left. \frac{\partial^2 \tilde{\omega}_1}{\partial \Phi^2} \right|_{\Phi \rightarrow \Theta} \right), \quad (5)$$

then in the frame rotating at ω_Φ , excluding oscillating terms which time-average to zero, the Hamiltonian is a perfect iSWAP (Eq. (7) of the main text). Because the measurement frame rotates at the $\delta = 0$ dressed frequencies, $\tilde{\omega}_1(\Theta)$ and $\tilde{\omega}_2(\Theta)$, the qubits pick up an additional phase during the iSWAP with respect to the measurement frame. This phase is

compensated after by applying single qubit Z gates.

To further understand the behavior of the gate as a function of the system parameters, we perform a numerical analysis of the whole system, consisting of three charge-coupled anharmonic transmon devices in a line where the middle transmon is flux-tunable (tunable bus). The Hamiltonian for this system of transmons, modeled as Duffing oscillators (truncated to three levels in the calculation), is given by

$$\begin{aligned}
H_N = & \sum_{i=1}^2 \left[\omega_i a_i^\dagger a_i + \frac{\alpha_i}{2} (1 - a_i^\dagger a_i) a_i^\dagger a_i \right] + \omega_{TB}(\Phi(t)) a_{TB}^\dagger a_{TB} + \frac{\alpha_i}{2} (1 - a_{TB}^\dagger a_{TB}) a_{TB}^\dagger a_{TB} \\
& + \sum_{i=1}^2 g_i (a_i^\dagger + a_i) (a_{TB}^\dagger + a_{TB}).
\end{aligned} \tag{6}$$

Note that Eq. (6) is the transmon generalization of Eq. (1) in the main text. Here we define creation (annihilation) operators for the i th fixed frequency qubit a_i^\dagger (a_i), with $0 - 1$ level transition energies ω_i and anharmonicities $\alpha_i = -E_{C_i}$ related to the charging energy of the i th qubit. Similar definitions are given for the tunable bus, with operators a_{TB}^\dagger (a_{TB}), and time-dependent frequency $\omega_{TB}(\Phi(t))$. The bus frequency as a function of flux is given by Eq. (2) of the main text and we assume a flux time-dependence of $\Phi(t) = \Theta + \delta \epsilon(t) \cos(\omega_\Phi t)$. The pulse shape $\epsilon(t)$ (range $[0, 1]$) is a square pulse with Gaussian edges with ramp-up/down time of ≈ 25 ns (same as the experiment).

For the calculation we work in the measurement basis obtained by numerically diagonalizing the time-independent Hamiltonian, $H_{N,0}$, given by Eq. (6) when $\omega_{TB}(\Phi(t)) = \omega_{TB}(\Theta)$. The unitary transformation to the measurement basis from $H_{N,0}$ is given by $U_{N,0}$. In a rotating frame at the dressed qubit frequencies the dynamics of the time-dependent flux pulse are described by the interaction Hamiltonian,

$$H_I(t) = U_I [\omega_{TB}(\Phi(t)) - \omega_{TB}(\Theta)] a_{TB}^\dagger a_{TB} U_I^\dagger, \tag{7}$$

$$U_I = e^{-i(U_{N,0}^\dagger H_{N,0} U_{N,0})t} U_{N,0}. \tag{8}$$

The flux pulse parameters used for the simulation are calibrated numerically by evolving the state $|01\rangle$ by H_I for a fixed gate time to state $|\Psi\rangle$ and optimizing the overlap $|\langle\Psi|10\rangle|^2$ (1 for a perfect iSWAP), as a function of the drive amplitude δ and drive frequency ω_Φ . An example of the numerical calibration is plotted in (a) of Fig. 3 for a gate time of 190 ns, where the optimal operational point is found at $\delta = 0.164$, $\omega_\Phi - \Delta\tilde{\omega}(\Theta) = 2\pi \times -3.7$ MHz.

The additional phases on the qubits in the measurement frame (as discussed in the previous paragraph) are also numerically calibrated.

Using this procedure, we calibrate the gate for different gate times and then include decoherence effects by solving a master equation for the density matrix of the system

$$\dot{\rho} = -i[H_I, \rho] + \sum_{i=1}^2 \left[\Gamma_{-,i}^{DC} \mathcal{D}[\sigma_i^-] \rho + \frac{\Gamma_{\phi,i}^{DC}}{2} \mathcal{D}[\sigma_i^Z] \rho \right], \quad (9)$$

where we have defined the decay and dephasing rates $\Gamma_{-,i} = 1/T_{1,i}^{DC}$, $\Gamma_{\phi,i}^{DC} = 1/T_{2,i}^{DC}$ through the values measured at the DC flux bias points on the i th qubit (see Fig. 4). The super-operator $D[\hat{O}]\rho$ is defined in the standard way, $D[\hat{O}]\rho = (2\hat{O}\rho\hat{O}^\dagger - \hat{O}^\dagger\hat{O}\rho - \rho\hat{O}^\dagger\hat{O})/2$. The effective damping and Z operators σ_i^- , σ_i^Z are defined in the measurement basis for the first two levels of the transmon qubits. For each gate time we compute the average gate fidelity

$$F = \int d|\Psi\rangle \text{Tr}[\rho_{|\Psi\rangle} U_{\text{iSWAP}} \rho_{|\Psi\rangle}] \quad (10)$$

where $\rho_{|\Psi\rangle}$ is the resulting density matrix after evolving Eq. (9) with input state $|\Psi\rangle$ and U_{iSWAP} is the ideal iSWAP gate. The results for the gate error $1 - F$ are shown in (b) of Fig. 3. We observe an optimal gate time range around ≈ 150 ns: for shorter gate times the fidelity is limited by leakage to the coupler and higher transmon levels, while for longer times decoherence imposes a lower bound on gate error. Experimentally measured gate errors, plotted on top of the simulation results are consistent with this optimal gate time. There may be additional sources of error in the actual experiment such as $1/f$ flux noise and coupler losses, which are not considered in this calculation.

To estimate leakage, we evolve according to H_I starting in the four basis states $|00\rangle, |01\rangle, |10\rangle, |11\rangle$ and compute the population in higher excited states after the gate. At short gate times, leakage is a considerable issue, but it becomes negligible as the gate time increases past ≈ 140 ns. The simulation results are shown in (c) of Fig. 3.

III. SINGLE QUBIT COHERENCE AND RB

As discussed in the main text and in § II of this supplement, the dressed qubits are weakly flux-tunable as given by Eq. (1). Flux noise on the tunable bus can therefore cause dephasing of the qubits. In Ref.¹, the relationship between T_2^* and flux noise for noise power

of the form $S(f) = A^2/f$, is given by the expression

$$T_2^* = \frac{1}{A} \left| \frac{\partial \omega}{\partial \phi} \right|^{-1}, \quad (11)$$

$$= \frac{1}{A} \left| \frac{g^2}{\Delta} \frac{\partial \omega_{TB}}{\partial \phi} \right|^{-1}. \quad (12)$$

To measure flux noise in our experiment we plot T_2^* versus the slope of the flux tuning curve in (c) of Fig. 4. We fit the data to the function,

$$T_2^* = \frac{1}{\gamma_0 + \gamma_1 \partial \nu_{TB} / \partial \phi}, \quad (13)$$

where γ_0 accounts for decoherence from all other sources and γ_1 is the prefactor of Eqn. 12. From the fit we get that $A = 2.2 \times 10^{-4} \Phi_0$. We also measure T_1 and T_2 (echo) times for each of the qubits as a function of the DC flux. In the range measured, these quantities are not a function of flux so we infer that there is no strong Purcell effect from the coupler and that the flux noise is predominantly low frequency.

To further characterize our single qubit gates we perform randomized benchmarking (RB) of the fixed-frequency qubits with the tunable bus qubit bias at $\phi = -0.108\phi_0$ (the flux bias for our two-qubit gate). This data is shown in (a) of Fig. 5. We perform standard RB, where each RB experiment is run separately, and simultaneous RB, where the RB experiments and qubit measurements are performed at the same time. Simultaneous RB characterizes the level of crosstalk and spurious interaction between the qubits. As shown in (b) of Fig. 5 the spurious ZZ interaction is small at this flux bias (66kHz). Combined with the large detuning between our qubits this means that crosstalk is low and so the fidelity from simultaneous and standard RB are the same; the fidelities are 0.99905(2) and 0.99947(1) for qubits 1 and 2 respectively.

IV. ADDITIONAL CHARACTERIZATION OF THE ISWAP GATE

In the main text, we described the implementation of our two-qubit iSWAP gate. Here we detail some additional characterizations of that gate. In (b) of Fig. 3 we show data for the gate fidelity from randomized benchmarking (RB) as a function of gate length. We provide two measurements of the RB fidelity; one by measuring the ground state of qubit 1 (tracing over qubit 2) and the other by measuring the ground state of qubit 2. It should be emphasized that these are from the same experiment, i.e. we perform a set of two-qubit

Cliffords using the iSWAP gate as a primitive and then measure the average state of both qubit 1 and qubit 2 simultaneously. RB theory predicts that these measurements should give the same value for the fidelity since the random Clifford sequences mix errors equally to both qubits. However, we see a slight discrepancy between these channels that increases as we go to shorter gate times. The source of said discrepancy is an ongoing investigation. Nevertheless, both measures of fidelity show the same trend; there is an optimal fidelity at approximately 180 ns and fidelity decreases away from that point for both shorter and longer gates. This is consistent with our numerical calculation in § II which is also shown on the plot.

Another possible error as we drive harder is leakage out of the computational subspace. There are primarily two paths for leakage with this type of gate. The first path is a direct sideband drive from $Q1$ or $Q2$ to the tunable bus. This is a first-order process but is strongly off-resonance by ensuring that $|\Delta_{i,TB}| \gg |\Delta_{12}|$. The second path is from $|11\rangle \rightarrow |20\rangle, |20\rangle$ since there is also an exchange coupling between these states. The detuning of this transition compared to the wanted swap transition is,

$$|2\omega_{1/2} - E_{C,1/2} - (\omega_1 + \omega_2)| - |\omega_1 - \omega_2|, \quad (14)$$

$$|\omega_{1/2} - \omega_{2/1} - E_{C,1/2}| - |\omega_1 - \omega_2|. \quad (15)$$

For large detuning compared to the anharmonicity this transition is off-resonant by the anharmonicity, which is large compared to the swap rate. For example in our sample $|\omega_1 - \omega_2|/2\pi = 854$ MHz and $|\omega_1 - \omega_2 - E_{C1}|/2\pi = 530$ MHz ($E_{C1}/2\pi = 324$ MHz) and $|\omega_2 - \omega_1 - E_{C2}|/2\pi = 1089$ MHz ($E_{C2}/2\pi = 235$ MHz). To characterize leakage experimentally we perform a variation of the RB process. First, we perform standard two-qubit RB and measure the average state of both qubits. The value measured on qubit 1 (normalized so that $|0\rangle$ is 1 and $|1\rangle$ is 0) is $\rho_{00} + \rho_{01} + \xi_1$ where ξ_1 represents leakage. Next, we repeat the same experiment with a π -pulse at the end so that the measured state is now $\rho_{10} + \rho_{11} + \xi_1$ where ρ is the density matrix just before the π -pulse and ξ is unchanged by the pulse. Adding both qubits and measurements together we get,

$$\begin{aligned} & (\rho_{00} + \rho_{01} + \xi_1) + (\rho_{00} + \rho_{10} + \xi_2) + (\rho_{10} + \rho_{11} + \xi_1) + (\rho_{01} + \rho_{11} + \xi_2) \\ & = 2(\text{tr}(\rho) + \xi_1 + \xi_2). \end{aligned} \quad (16)$$

The exact values of ξ_1, ξ_2 are unknown because they depend on the leakage states, however, under the assumption they cause a deviation in the measurement signal we can look at this

measure as a function of the RB sequence length to observe leakage trends. In (a) of Fig. 6 we illustrate this leakage measurement. Typical data asymptotes away from one and we can define such an asymptote to represent a leakage metric. Plotting the leakage metric versus gate length we see that there is no strong evidence of leakage that is increasing as we decrease the gate length. Our numerical calculation of leakage in (c) of Fig. 3 predicts large leakage at sufficiently short gates, but these are beyond our measured range.

Gate errors are not only the result of incoherent noise. There are also coherent errors, e.g., due to phase and/or amplitude errors. To characterize these errors we perform purity RB as shown in (b) of Fig. 6. Here we plot the trace of ρ^2 which measures the coherence of the density matrix (a pure state should be $Tr(\rho^2) = 1$). Assuming pure depolarizing noise $1 - \alpha$ the density matrix after n Cliffords is,

$$\rho(n) = \alpha^n \rho_0 + (1 - \alpha^n) \frac{\mathcal{I}}{d}, \quad (17)$$

$$\rho^2(n) = \alpha^{2n} \rho_0^2 + (1 - \alpha^n)^2 \frac{\mathcal{I}}{d^2} + 2\alpha^n (1 - \alpha^n) \frac{\rho_0}{d}, \quad (18)$$

$$\text{Trace}(\rho^2(n)) = \alpha^{2n} + \frac{(1 - \alpha^n)^2}{d} + \frac{2\alpha^n (1 - \alpha^n)}{d}, \quad (19)$$

$$= \left(1 - \frac{1}{d}\right) \alpha^{2n} + \frac{1}{d}. \quad (20)$$

$$(21)$$

Therefore we fit we fit the curve to a form $\text{Trace}(\rho^2) = A\alpha^{2n} + B$ where n is the number of Cliffords. We can compare the pure dephasing error from this fit (per two-qubit primitive), $\epsilon = 3/4(1 - \alpha^{2/3})$, to that of standard RB. This procedure gives a “purity error” of 2.2%, comparable to our gate error, demonstrating that our gate is dominated by incoherent errors. We also performed full quantum process tomography (QPT) on the gate as shown in Fig. 7. The fidelity from QPT is 0.949 from maximum likelihood estimation and 0.96 from the raw linear inversion. While QPT gives a full description of the gate it is susceptible to state preparation and measurement (SPAM) errors.

REFERENCES

- ¹J. Koch, T. M. Yu, J. Gambetta, A. A. Houck, D. I. Schuster, J. Majer, A. Blais, M. H. Devoret, S. M. Girvin, and R. J. Schoelkopf, Phys. Rev. A **76**, 042319 (2007).

FIGURES

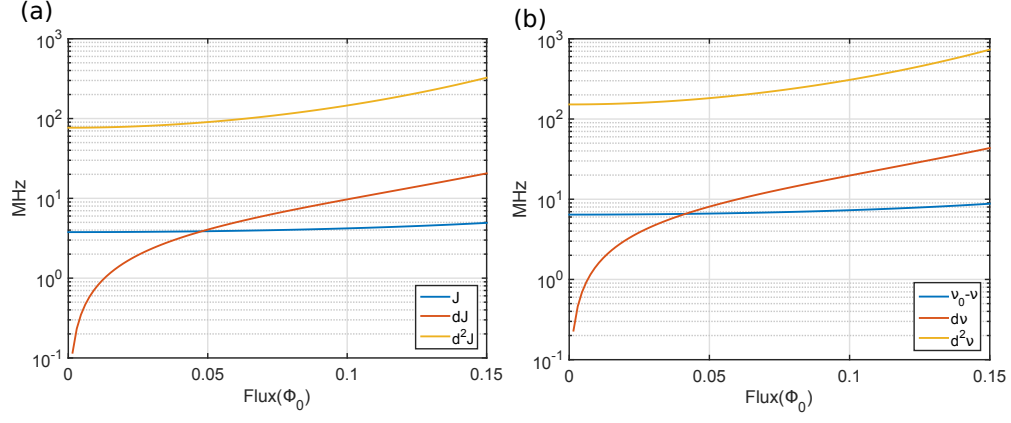


FIG. 2. Numerical calculation of (a) J , $\partial J/\partial\Phi$, $\partial^2 J/\partial\Phi^2$ and (b) $\tilde{\nu}_1 - \nu_1$, $\partial\tilde{\nu}_1/\partial\Phi$, $\partial^2\tilde{\nu}_1/\partial\Phi^2$ ($2\pi\nu = \omega$) versus DC flux for the parameters of our device.

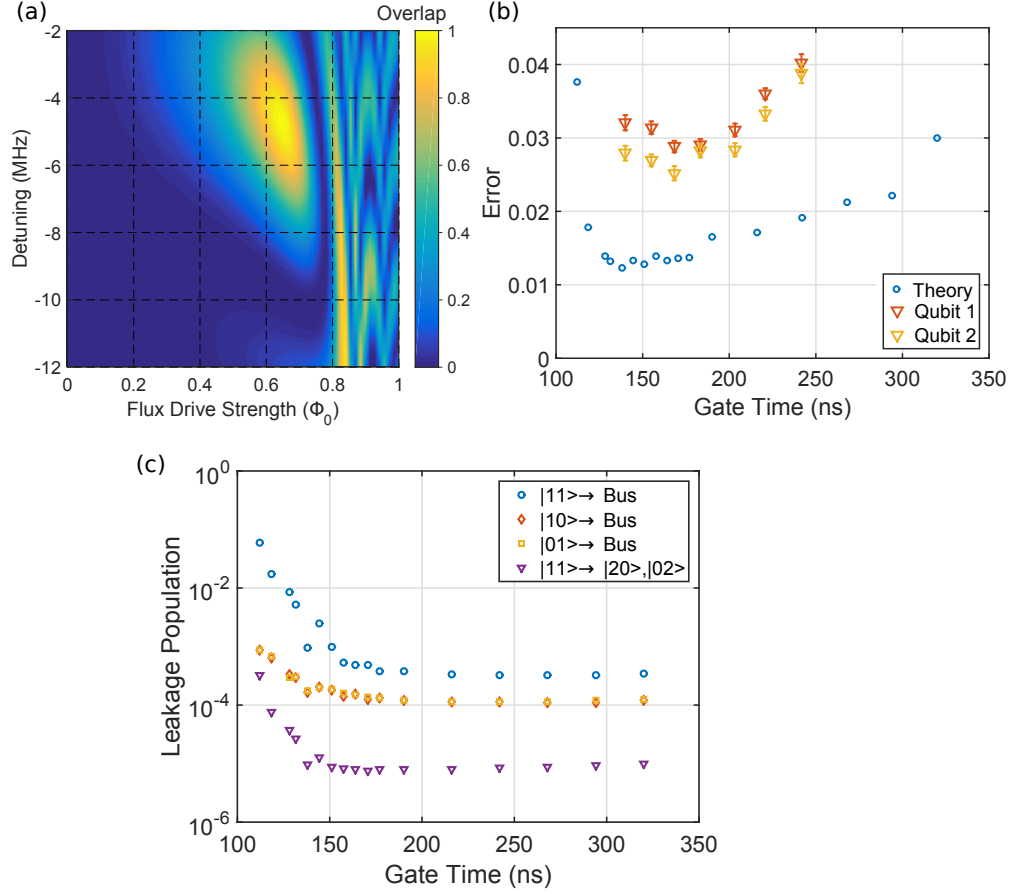


FIG. 3. (a) Numerical optimization of $|\langle\Psi|10\rangle|^2$ where $|\Psi\rangle$ is the calculated state after the gate starting in $|01\rangle$ versus the swap drive frequency (detuned from the dressed qubit detuning for $\delta = 0$) and drive strength for a gate length of 190 ns. (b) Gate error vs gate time calculated numerically (circle) versus experiment (triangles). (c) Calculated leakage out of the computational subspace versus gate length. Most of the leakage is into the tunable bus.

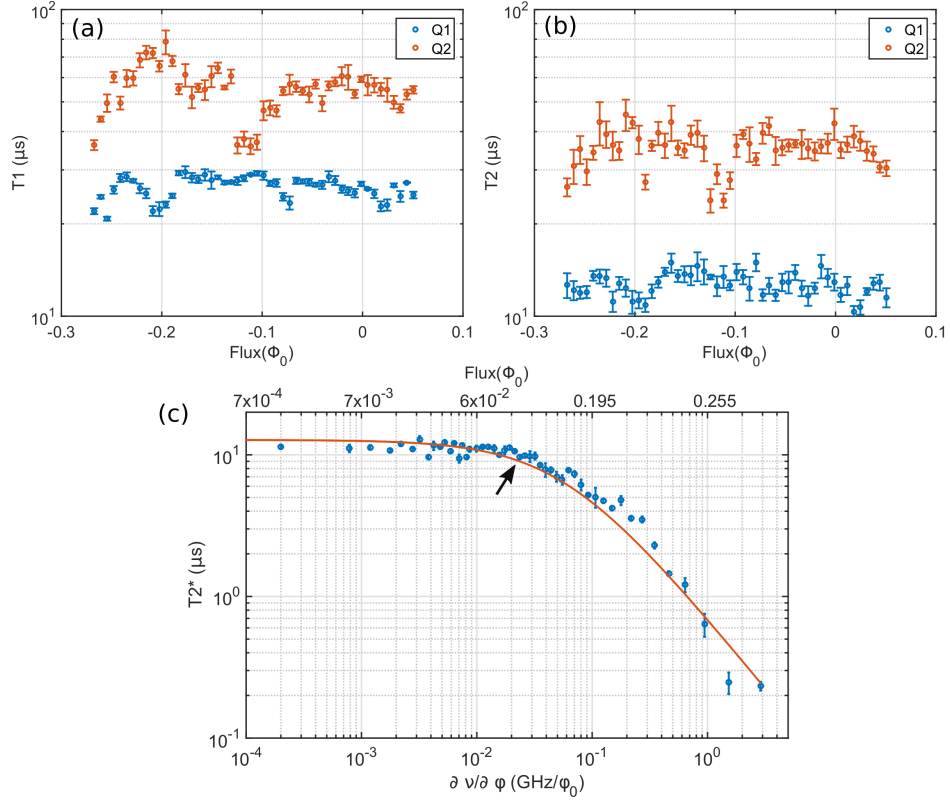


FIG. 4. Single qubit coherence measurements. (a) T_1 and (b) T_2 (echo) for both qubits as a function of the DC flux applied to the tunable bus qubit. (c) Qubit 1 T_2^* as a function of the slope of the tunable bus tuning curve at specific DC flux points. The arrow indicates the point where we perform our two-qubit gate.

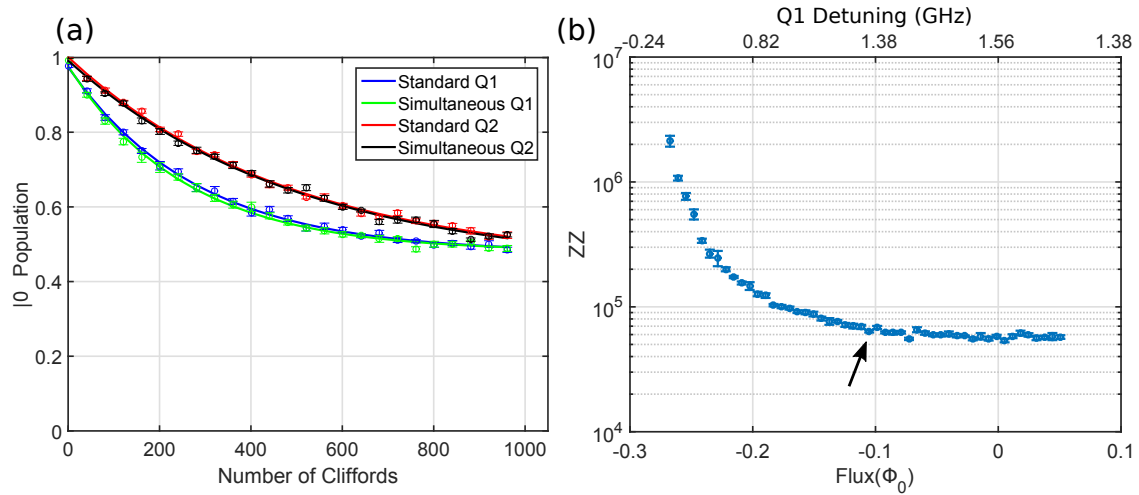


FIG. 5. (a) Standard and simultaneous RB for qubits 1 and 2 taken at the flux bias used for our two-qubit gate described in the main text. (b) ZZ Measurement as a function of DC flux bias. The arrow indicates the flux bias for our gate. For moderate detuning between qubit 1 and the tunable bus qubit (qubit 2 is always more detuned) the ZZ is low and comparable to the calculated rate of 25kHz at $\phi = 0$. The ZZ rate increases for larger flux bias as qubit 1 and the tunable bus move into resonance.

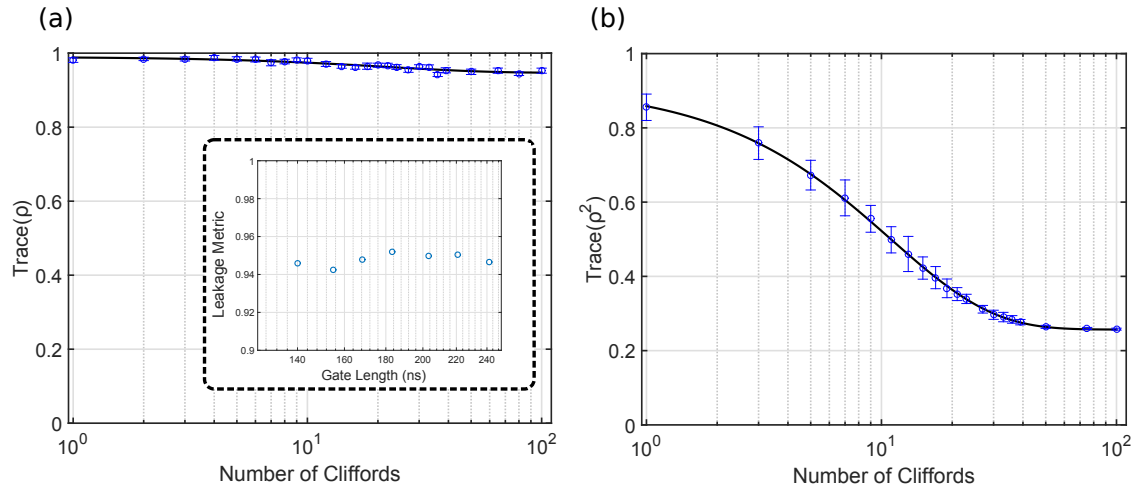


FIG. 6. (a) Typical leakage RB data as a function of the RB sequence length. This data is for the gate length used for the gate presented in the main text. (Inset) is the leakage metric (the asymptote of the RB data) versus gate length. (b) Purity RB for the gate length used in the main text.

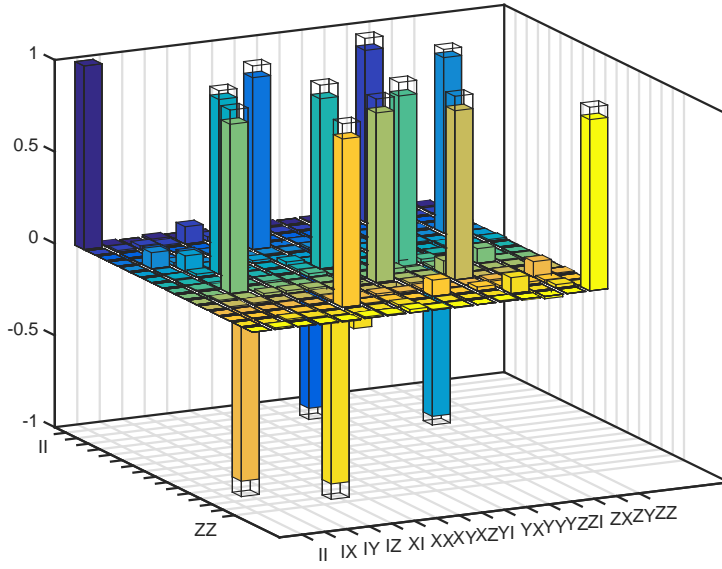


FIG. 7. Quantum process tomography (QPT) of the iSWAP gate in the Pauli transfer matrix representation. The wireframe bars represent the ideal values of the coefficients (ideally there are only ± 1 and 0 valued elements).